Theor Chem Acc (2012) 131:1153
DOI 10.1007/s00214-012-1153-7

REGULAR ARTICLE

Recent applications and developments of charge equilibration force fields for modeling dynamical charges in classical molecular dynamics simulations

Brad A. Bauer · Sandeep Patel

Received: 12 May 2011 / Accepted: 27 September 2011 / Published online: 2 March 2012

Abstract With the continuing advances in computational hardware and novel force fields constructed using quantum mechanics, the outlook for non-additive force fields is promising. Our work in the past several years has demonstrated the utility of polarizable force fields, in our hands those based on the charge equilibration formalism, for a broad range of physical and biophysical systems. We have constructed and applied polarizable force fields for small molecules, proteins, lipids, and lipid bilayers and recently have begun work on carbohydrate force fields. The latter area has been relatively untouched by force field developers with particular focus on polarizable, non-additive interaction potential models. In this review of our recent work, we discuss the formalism we have adopted for implementing the charge equilibration method for phase-dependent polarizable force fields, lipid molecules, and small-molecule carbohydrates. We discuss the methodology, related issues, and briefly discuss results from recent applications of such force fields.

Keywords Force field · Molecular dynamics simulations · Quantum mechanics · Polarizable · Charge equilibration

Published as part of the special collection of articles: From quantum mechanics to force fields: new methodologies for the classical simulation of complex systems.

B. A. Bauer · S. Patel (✉)
Department of Chemistry and Biochemistry,
University of Delaware, Newark, DE 19716, USA
e-mail: sapatel@udel.edu

1 Introduction

Computational chemistry is an indispensable tool in the arsenal of today's chemist, biochemist, and biologist. It is thus not surprising that the computational modeling community continues to push for advanced methods and models at a feverish pace. The advances have become ever faster in the recent decades due to the increased computational resources emerging as high-performance computer hardware becomes available to the masses at commodity prices. Along with the advances in hardware and software, algorithmic and force field developments have impacted the state-of-the-art profoundly. Though the issues of sampling on accurate (free) energy surfaces are intimately coupled, work continues along both fronts fairly along independent lines, largely due to the fact that both problems are profoundly difficult to tackle simultaneously with current resources. This review article deals with the aspect of molecular interaction models, and in particular, models based on non-additive electrostatic interactions. For the purposes of this review, we consider non-additive electrostatic models as those that allow for the variation of the local molecular electrostatic environment (i.e., charges, dipole moments, and higher-order electrostatic moments) based on some pre-defined, systematic theoretical formalism. Work in the recent decades has realized the need to revisit the implications of electrostatic polarizability in defining the quality of molecular simulations. As a result, the development of models that explicitly model polarizability has been steadily progressing. Considering the formalisms for modeling molecular polarizability in a classical treatment, point-dipole (and higher-order multipole) [1–11], Drude oscillator [12–21], ab initio-inspired methods [10, 22–27], and charge equilibration/fluctuating charge [28–44] models are currently being developed.

A detailed comparison among these approaches is beyond the scope of the current work, although recent reviews have addressed such comparisons [45]. The charge equilibration approach, which is used extensively in this work, is discussed in detail in the next section. In general, polarization methods consider the induction of a dipole moment ($\boldsymbol{\mu}_{\text{ind}}$) in the presence of an electric field ($\mathbf{E}$):

$$\boldsymbol{\mu}_{\text{ind}} = \alpha \mathbf{E}. \tag{1}$$

These formalisms differ in the treatment of the polarizability, α. For the purposes of model development and parameterization, α is often determined empirically. There is not a consensus on the magnitude of α in the condensed phase for numerous molecular species. Consequently, the value of polarizability in some force fields is determined empirically. The nature of the condensed-phase polarizability is either treated in an ad hoc manner via scaling to reproduce certain target properties of condensed-phase and gas-phase cluster models. In other cases, the gas-phase polarizability is applied directly for models of the condensed phase; the parameters of the model then implicitly account for the variation of polarizability with environment (condensed phase versus gas phase).

2 Force fields

2.1 Charge equilibration force fields

We next consider details of the CHEQ method and considerations in our specific implementation of the method. An additive (or *non-polarizable*) formalism for force fields is based on the construct that all atomic partial charges are fixed throughout the course of the simulations. Alternatively, we can consider the variation of atomic partial charge using the charge equilibration (CHEQ) formalism [28–37, 39]. The CHEQ formalism is based on Sanderson's idea of electronegativity equilibration [28, 29] in which the chemical potential is equilibrated via the redistribution of charge density. In a classical sense, charge density is reduced to partial charges, Q_i on each atomic site i. The charge-dependent energy for a system of M molecules containing N_i atoms per molecule is then expressed as

$$E_{\text{CHEQ}}(\vec{R},\vec{Q}) = \sum_{i=1}^{M}\sum_{\alpha=1}^{N}\chi_{i\alpha}Q_{i\alpha} + \frac{1}{2}\sum_{i=1}^{M}\sum_{j=1}^{M}\sum_{\alpha=1}^{N_i}\sum_{\beta=1}^{N_j}J_{i\alpha j\beta}Q_{i\alpha}Q_{j\beta} + \frac{1}{2}\sum_{i=1}^{MN'}\sum_{j=1}^{MN'}\frac{Q_iQ_j}{4\pi\epsilon_0 r_{ij}} + \sum_{j=1}^{M}\lambda_j\left(\sum_{i=1}^{N}Q_{ji} - Q_j^{\text{Total}}\right) \tag{2}$$

where the χ terms represent the atomic electronegativities that control the directionality of electron flow and J terms represent the atomic hardnesses that control the resistance to electron flow to or from the atom. Although these parameters are derived from the definitions of electron affinity and ionization potential, they are treated as empirical parameters for individual atom types. Heterogeneous hardness elements that describe the interaction between two different atom types are calculated using the combining rule [46] on the parameterized homogeneous hardness elements (J_{ii}°):

$$J_{ij}(R_{ij}, J_{ii}^{\circ}, J_{jj}^{\circ}) = \frac{\frac{1}{2}\left(J_{ii}^{\circ} + J_{jj}^{\circ}\right)}{\sqrt{1.0 + \frac{1}{4}\left(J_{ii}^{\circ} + J_{jj}^{\circ}\right)^2 R_{ij}^2}} \tag{3}$$

where R_{ij} is the distance between atoms i and j. This combination locally screens Coulombic interactions but provides the correct limiting behavior for atomic separations greater than approximately 2.5 Å. The standard Coulomb interaction between sites not involved in the dihedral, angle, or bonded interactions (indicated by primed summation) with each other is included as the third term in Eq. 2. The second term in Eq. 2 represents the local charge transfer interaction, which is usually restricted to within a molecule or an appropriate charge normalization unit, that is, no intermolecular charge transfer. Charge is constrained via a Lagrange multiplier, λ, which is included for each molecule as indicated in the last term of Eq. 2. We remark that use of multiple charge normalization units can modulate molecular polarizability by limiting intramolecular charge transfer to physically realistic distances. Such an approach controls previously observed superlinear polarizability scaling [41, 43, 47], which also manifests as the polarization catastrophe (as observed in point polarizable force fields) [8, 41], while developing a construct for piecing together small molecular entities into macromolecules.

Charge degrees of freedom are propagated via an extended Lagrangian formulation imposing a molecular charge neutrality constraint, thus providing for electronegativity equilibration at each dynamics step. The system Lagrangian is:

$$L = \sum_{i=1}^{M}\sum_{\alpha=1}^{N}\frac{1}{2}m_{i\alpha}\left(\frac{\mathrm{d}r_{i\alpha}}{\mathrm{d}t}\right)^2 + \sum_{i=1}^{M}\sum_{\alpha=1}^{N}\frac{1}{2}m_{Q,i\alpha}\left(\frac{\mathrm{d}Q_{i\alpha}}{\mathrm{d}t}\right)^2 - E(Q,r) - \sum_{i=1}^{M}\lambda_i\sum_{\alpha=1}^{N}Q_{i\alpha} \tag{4}$$

where the first two terms represent the nuclear and charge kinetic energies, the third term is the potential energy, and the fourth term is the molecular charge neutrality constraint enforced on each molecule i via a Lagrange multiplier λ_i. The fictitious charge dynamics are determined using a charge "mass" with units of (energy time^2/charge^2). This is

analogous to the use of an adiabaticity parameter in fictitious wavefunction dynamics in Car Parinello (CP) type methods [31, 48]. Charges are thus propagated based on the forces arising from differences between the average electronegativity of a molecule and the instantaneous electronegativity at an atomic site.

2.2 Polarizability in charge equilibration models

When the electrostatic energy expression for a single molecule comprised of N atoms is differentiated with respect to charge and set equal to zero,

$$\frac{\partial E}{\partial Q_i} = \chi_i^0 + J_{ii}^{\circ} Q_i + \sum_{j \neq i}^{N} J_{ij} Q_j = 0, \tag{5}$$

a set of N equations can be solved to determine the set of charges minimizing the energy. In matrix form, this set of equations can be recast as

$$\mathbf{JQ} = -\boldsymbol{\chi} \tag{6}$$

where $\mathbf{J}$ is the atomic hardness matrix, $\mathbf{Q}$ is the atomic charge vector, and $\boldsymbol{\chi}$ is the atomic electronegativity vector. Written explicitly, the matrix representation is:

$$\begin{bmatrix} J_{11} & J_{12} & \cdots & \cdots & J_{1N} \\ J_{21} & \ddots & & & \vdots \\ \vdots & & \ddots & & \vdots \\ \vdots & & & \ddots & \vdots \\ J_{N1} & \cdots & \cdots & \cdots & J_{NN} \end{bmatrix} \begin{bmatrix} Q_1 \\ Q_2 \\ \vdots \\ \vdots \\ Q_N \end{bmatrix} = - \begin{bmatrix} \chi_1 \\ \chi_2 \\ \vdots \\ \vdots \\ \chi_N \end{bmatrix}. \tag{7}$$

These equations can be augmented to include the charge conservation constraint,

$$\sum_{i=1}^{M} Q_i = Q_{\text{net}}, \tag{8}$$

to produce a modified set of equations:

$$\mathbf{J}'\mathbf{Q}' = -\boldsymbol{\chi}'; \tag{9}$$

this is written explicitly as:

$$\begin{bmatrix} J_{11} & J_{12} & \cdots & \cdots & J_{1N} & 1 \\ J_{21} & \ddots & & & \vdots & 1 \\ \vdots & & \ddots & & \vdots & \vdots \\ \vdots & & & \ddots & \vdots & \vdots \\ J_{N1} & \cdots & \cdots & \cdots & J_{NN} & 1 \\ 1 & \cdots & \cdots & \cdots & 1 & 0 \end{bmatrix} \begin{bmatrix} Q_1 \\ Q_2 \\ \vdots \\ \vdots \\ Q_N \\ \lambda \end{bmatrix} = - \begin{bmatrix} \chi_1 \\ \chi_2 \\ \vdots \\ \vdots \\ \chi_N \\ Q_{\text{net}} \end{bmatrix} \tag{10}$$

In Eq. 10, we have enforced the constraint that charge is conserved within the molecule, or equivalently, that the sum of atomic partial charges equals the desired net charge. As alluded to in the previous section, it is appropriate to limit the extent of intramolecular charge transfer by introducing additional charge constraints. For instance, the total charge of the molecule is constrained to Q_{net} while additionally requiring the sum of charges for a subset of atoms within the molecule to equal a specified quantity, Q_{net}, k. We refer to this subset of atoms as a charge conservation unit. Since the net charge over the entire molecule must be maintained, the following condition must hold:

$$Q_{\text{net}} = \sum_{k=1}^{M} Q_{\text{net},k}, \tag{11}$$

in which M denotes the number of charge conservation units. We can expand our previous illustration of the system of equations generated with a single charge constraint (Eq. 10) to show the set of equations when a molecule is broken into two charge conservation units:

$$\begin{bmatrix} J_{11} & \cdots & J_{1h} & J_{1(h+1)} & \cdots & J_{1N} & 1 & 0 \\ \vdots & \ddots & & & & \vdots & \vdots & \vdots \\ J_{h1} & & J_{hh} & & & \vdots & 1 & 0 \\ J_{(h+1)1} & & & J_{(h+1)(h+1)} & & \vdots & 0 & 1 \\ \vdots & & & & \ddots & \vdots & \vdots & \vdots \\ J_{N1} & \cdots & J_{Nh} & J_{N(h+1)} & \cdots & J_{NN} & 0 & 1 \\ 1 & \cdots & 1 & 0 & \cdots & 0 & 0 & 0 \\ 0 & \cdots & 0 & 1 & \cdots & 1 & 0 & 0 \end{bmatrix} \begin{bmatrix} Q_1 \\ \vdots \\ Q_h \\ Q_{h+1} \\ \vdots \\ Q_N \\ \lambda_1 \\ \lambda_2 \end{bmatrix} = - \begin{bmatrix} \chi_1 \\ \vdots \\ \chi_h \\ \chi_{h+1} \\ \vdots \\ \chi_N \\ Q_{\text{net},1} \\ Q_{\text{net},2} \end{bmatrix}. \tag{12}$$

For this example, atomic sites 1 through h are grouped into one charge conservation unit, while atomic sites $h + 1$ through N are grouped into a second charge normalization unit. In the augmented atomic hardness matrix, values of 1 in element (i, $N + 1$) or ($N + 1$, i) denote that atom i is assigned to the first charge conservation unit (which has a net charge of Q_{net}, 1). Similarly, values of 1 in elements (i, $N + 2$) or ($N + 2$, i) denote that atom i is assigned to the second charge conservation unit (with net charge Q_{net}, 2).

The molecular polarizability in the CHEQ formalism can be calculated as [41]:

$$\alpha_{\gamma\beta} = \mathbf{R}_{\beta}^{T}\mathbf{J}'^{-1}\mathbf{R}_{\gamma} \quad (13)$$

where $\mathbf{J}'$ is the atomic hardness matrix augmented with the appropriate rows and columns to treat the charge conservation constraints. $\mathbf{R}_{\gamma}$ and $\mathbf{R}_{\beta}$ are the γ and β Cartesian coordinates of the atomic position vectors (which are also augmented to appropriately match the dimensions of the atomic hardness matrix).

3 Phase-dependence of molecular polarizability

A variety of recent theoretical investigations involving ab initio calculations with polarizable continuum solvent, the partitioning of cluster polarizabilities, and the temperature/density dependence of dielectric constants of fluids reasonably establish that the surrounding condensed-phase environment can significantly affect the polarizability of a solvated molecule. Krishtal et al. have previously reported that the average intrinsic polarizability of water molecules decreases as the size of a cluster increases and also as the number and type of hydrogen bonds on a molecule increases [49]. The notion of decreasing polarizability in condensed regions is further supported by the ab initio calculations of Morita involving water clusters [50] that suggest that the condensed-phase polarizability of water should be 7–9% lower than that of the gas-phase value. The spatial constraints imposed by condensed-phase environments limit the number of accessible excited states and diffuse character of the electron density distribution as dictated by Pauli's exclusion principle [20, 50]. A recent study by Schropp and Tavan [51] further suggests that the average effect of the inhomogeneous electric fields *within* the molecular volume of a single water molecule is consistent with classical parameterizations of polarizable water force fields in which the molecular polarizability is assigned a value around 68% of the gas-phase value. Our lab has also explored qualitatively the nature of intrinsic molecular polarizability and its reduction for water and monovalent halide anions using a cluster-based approach coupled with Hirshfeld partitioning [52]. Acknowledging that our approach does not consider explicitly effects of intermolecular charge transfer, we observe 40–50% reduction of the gas-phase intrinsic molecular polarizability of anions; the results of this study, along with the studies mentioned above, suggest that the exact absolute value of polarizability reduction in the condensed phase is still an unresolved issue. While these results suggest a reduction of polarizability within the condensed phase, the implications for the rate and nature of the decrease remain unclear. Similarly, a self-consistent analytic formalism capable of correlating changes in molecular polarizability to atomic or molecular properties remains undetermined. While it has been observed that metrics such as aggregation number, hydrogen bonding, or local density are associated with a phase-dependent decrease in molecular polarizability, such metrics are impractical from the perspective of a molecular dynamics simulation. Consequently, a relationship between the polarizability and an atomic property that smoothly and monotonically transitions from one phase to another is desirable in establishing a simple functional form for polarizability change between phases.

One potentially useful parameter for modeling phase-dependent changes in polarizability is the dipole moment of the molecule. Both experiment and theoretical calculations such as ab initio molecular dynamics simulations demonstrate water's molecular dipole moment increases moving from gas phase to condensed-phase environments [53–55]; currently, there is no consensus on an exact value of the average condensed-phase dipole moment of water. Molecular dipole moment can be readily calculated from classical molecular dynamics simulations from the atomic positions and partial charges. If a rigid water geometry is chosen, the calculation is even further simplified in that the dipole moment depends solely on the magnitude of the associated atomic partial charges. Furthermore, atomic hardnesses determine molecular polarizability within the charge equilibration formalism. Thus, a plausible approach to modeling a phase-dependent polarizability in water lies in coupling the atomic charges to the atomic hardness parameters. A similar approach has been previously implemented by Rappé and Goddard [30] for the hydrogen atom in which a linear charge dependence is introduced into the corresponding atomic hardness value. Most generally, each atomic hardness function will depend simultaneously on all partial charges within the molecule; however, a simpler approach (as adopted in our work) entails modulating or scaling all of the atomic hardness values within a molecule using a single parameter based on the polarization state of the molecule. Since the average molecular dipole moment for water appears to be correlated with the magnitude of the negative partial charge on the oxygen atom, we simplify our model by coupling the atomic hardnesses directly to the oxygen partial charge (carried by a lonepair *M*-site).

As can be inferred from Eq. 13, polarizability for a rigid water molecule within the CHEQ formalism (such as TIP4P-FQ [31]) is influenced by the magnitude of the atomic hardnesses. We introduce charge-dependent polarizability by establishing a charge dependence in the atomic hardness elements:

$$\mathbf{J}(Q_M) = g(Q_M)\mathbf{J}. \quad (14)$$

where $g(Q_M)$ is an imposed scaling function dependent on the *M*-site charge. In order to maintain proper gas and condensed-phase charge distributions, it is also necessary

to scale the electronegativity values in addition to the hardnesses. While reasonable results may be obtained by employing the same scaling factor for both the electronegativities and the hardnesses, finer control of the condensed-phase dipole moment distribution is afforded by a tunable factor for the electronegativity scaling. Such flexibility also permits better control of the bulk dielectric constant that may be obtained from the average condensed-phase dipole moment [56]. We introduce an empirical χ-scaling

$$\boldsymbol{\chi}(Q_M) = \frac{g(Q_M)}{h(Q_M)}\boldsymbol{\chi} = [(1-p) + pg(Q_M)]\boldsymbol{\chi} \tag{15}$$

where p is an empirical parameter that controls the extent to which $\boldsymbol{\chi}$ is scaled relative to the hardness scaling function. For $p = 1$, the scaling on electronegativity values is equivalent to that in the hardnesses; similarly, a value of $p = 0$ would correspond to no scaling (i.e., a constant electronegativity with no charge-dependent scaling). The resulting charge-dependent, intramolecular CHEQ energy expression is then:

$$E(Q) = \sum_{i=1}^{N}\chi_i(Q_M)Q_i + \frac{1}{2}\sum_{i=1}^{N}J_{ii}^{\circ}(Q_M)Q_i^2 + \sum_{i<j}^{N}J_{ij}(Q_M)Q_iQ_j + \lambda\left(\sum_{i=1}^{N}Q_i - Q_{total}\right). \tag{16}$$

Unfortunately, the explicit introduction of a charge dependence into the molecular hardness matrix results in the additional complication that the polarizability expression in Eq. 13 is no longer exact. Consequently, the corresponding system of equations for the equilibrium charges (and polarizabilities) is now a non-linear system and must be solved by an iterative approach. In situations where the equilibrium charge distribution is not strongly perturbed by the implicit charge dependence, a slightly modified version of Eq. 13

$$\alpha_{\beta\gamma}(Q_M) \approx \frac{\alpha_{\beta\gamma}}{\xi(Q_M)} - \left(\frac{\nabla_M g(Q_M)\langle R_\beta|\mathbf{J}^{-1}(\mathbf{r})|\hat{\mathbf{M}}\rangle}{|g(Q_M)|^2 h(Q_M)}\right)\left[p\chi_M\langle R_\beta|\mathbf{J}^{-1}(r)|\hat{\mathbf{M}}\rangle + \frac{1}{2}\mu_\gamma\right] \tag{17}$$

is convenient for obtaining a leading-order approximation of the polarizability in the absence of a fully non-linear treatment [57]. In the above expression, $\alpha_{\beta\gamma}$ is the $\beta\gamma$-element of the gas-phase molecular polarizability tensor, $\nabla_M g(Q_M)$ is the derivative of the scaling function with respect to Q_M, $\mathbf{R}_\beta$ is the β-position vector, $\hat{\mathbf{M}}$ is a matrix that selects elements associated with the M-site (since we have chosen our hardness elements to only depend on the oxygen charge), and μ_γ is the γ-component of the dipole moment. We see the charge-dependent polarizability differs from the unscaled (gas-phase) value by a multiplicative factor $\xi(Q_M) = 1/[g(Q_M)h(Q_M)]$ and additive terms, which are related to the M-site hardness and dipole moment, respectively. These additive terms of equal magnitude and opposite sign are small compared to the first term and do not greatly influence $\alpha(Q_M)$. If we neglect the additive terms and consider the limit in which $p = 1$, Eq. 17 reduces to

$$\alpha_{\beta\gamma}(Q_M) \approx \frac{\alpha_{\beta\gamma}}{g(Q_M)} \tag{18}$$

from which it is clearly seen that $\alpha(Q_M)$ modulates the gas-phase polarizability via an inverse relationship with the scaling function, $g(Q_M)$. While Eq. 18 is effective for illustrative purposes, we have employed Eq. 17 for calculations of the condensed-phase polarizability.

With an explicit charge-dependent polarizability using a simple scaling function $g(Q_M)$, it is relevant to discuss the nature and form of this scaling function. While there is no formal theory connecting charge and polarizability, general trends provide guiding insight. In prior work, Rappé and Goddard [30] have employed atomic hardnesses that depend linearly on charge. In the context of molecular dynamics simulations, such an approach would necessitate some degree of charge bounding to prevent unfavorable over-polarization or under-polarization and to establish consistent polarizabilities in the gaseous and condensed phases. In light of this, we have chosen to employ an error function that applies constant scaling in the purely condensed-phase and gaseous regions and approximately linear scaling in the intermediate region. The use of the error function is also preferred as it allows smooth transitions between each region, which is necessary to avoid discontinuities in the forces. Thus, we choose a scaling function of the form

$$g(Q_M) = a - b\,\mathrm{erf}(c(d - Q_M)) \tag{19}$$

since it incorporates additional empirical parameters that can be utilized to model the desired relationship between polarizability and charge. Parameters a and b collectively define the polarizability at the gaseous and condensed-phase limits. The rate of polarizability change with charge for non-isolated molecules is controlled by c. Collectively, c and d describe the onset of scaling and the range of charges over which polarizability changes.

We apply the above methodology to design a water model capable of capturing the variation of molecular polarizability in different electrochemical environments. The resulting TIP4P-QDP model (Transferable Intermolecular Potential 4-Site with Charge-Depenedent Polarizability) is based on the application of the charge-dependent scaling function to the original TIP4P-FQ model. We retain the TIP4P-FQ geometry in the TIP4P-QDP model;

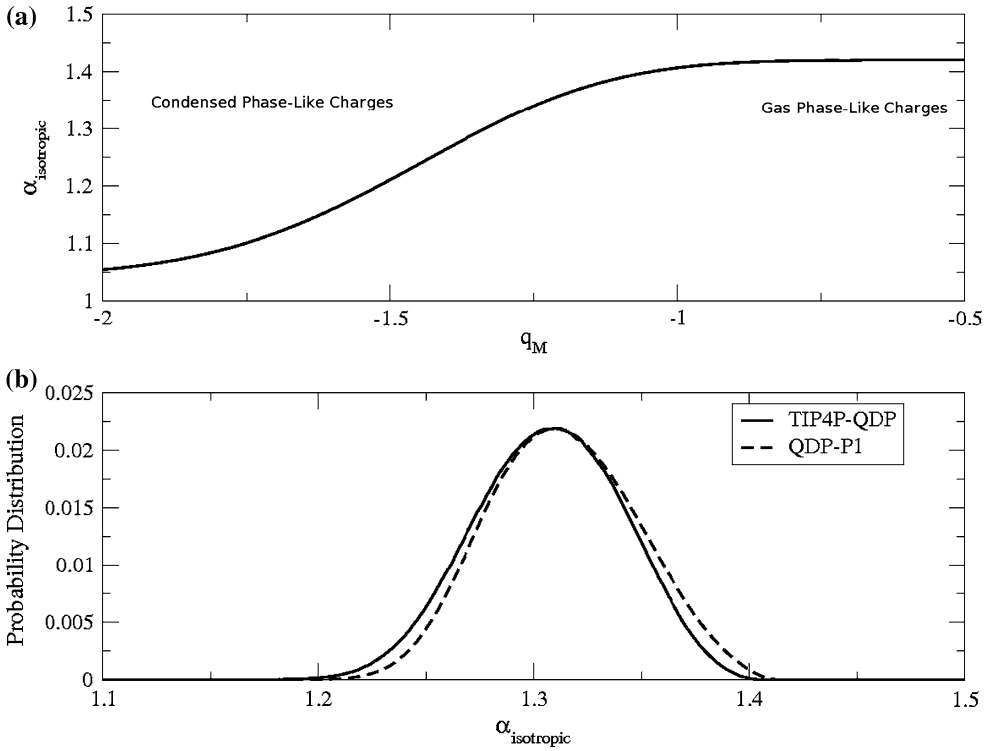

Fig. 1 Molecular polarizability scaling function and distribution for TIP4P-QDP and QDP-P1 water models. **a** Molecular polarizability (in Å^3) as a function of Q_M. **b** Distribution of molecular polarizabilities within the condensed phase. Polarizabilities were calculated using Eq. 17 and the charges from simulation. Data from Bauer et al. [57]

however, atomic hardnesses, electronegativities, and non-bonded parameters were adjusted to capture the desired physics associated with phase-dependent polarizability while reproducing target gas-phase and condensed-phase properties. Of primary interest, we reparameterize the hardness values to reproduce a reasonable gas-phase polarizability of 1.4 Å^3, which is notably higher than the empirical value offered by TIP4P-FQ ($\alpha \approx 1.12$ Å^3). We note that the resulting TIP4P-QDP gas-phase hardnesses maintain approximately the same relative magnitudes as the original TIP4P-FQ hardnesses. The error function form (Eq. 19) is then parameterized with the caveat that the gas-phase polarizability remains unchanged. In the condensed phase, the hardnesses are scaled by a value of $g(Q_M) > 1$ for charges greater than the equilibrium gas-phase charges. The parameters of the scaling function which influence the height, slope, and inflection are determined empirically such that the resulting polarizability distribution is centered about an appropriate condensed-phase polarizability value. For TIP4P-QDP, the average polarizability in the condensed phase is calculated to be 1.309 ($\pm$ 0.001) Å^3, approximately 17% higher than the static condensed-phase polarizability of TIP4P-FQ and about 11% less than the experimental gas-phase value. The average condensed-phase value approximately reflects a 6.5% reduction in the molecular polarizability relative to the TIP4P-QDP gas-phase value, which agrees well with the estimated range of 7–9% reduction calculated by Morita [50] from first principles. The scaling function allows for TIP4P-QDP molecules to have polarizabilities as low as 1.05 Å^3. The polarizability distribution observed in the condensed phase is presented in (Fig. 1), which was estimated from *M*-site charges taken from a condensed-phase simulation in conjunction with Eq. 17. This distribution exhibits a width of observed molecular polarizabilities of about 0.20 Å^3.

Regarding electronegativity scaling, a final value of the *p*-parameter is determined to be $p = 0.80$; this value generates a condensed-phase dipole moment distribution with an average of 2.641($\pm$ 0.001) Debye, similar to that exhibited by the TIP4P-FQ model. For further comparisons, a model consisting of full scaling $p = 1.0$ was also developed and parameterized. The results of this model (referred to as QDP-P1) are also included in this work as a reference in order to more fully clarify differences between the TIP4P-FQ and TIP4P-QDP models; QDP-P1 notably higher dipole moments in the condensed phase ($\langle\mu\rangle \approx$ 2.75), an anticipated consequence of scaling electronegativity and hardness equivalently. Introduction of the scaling function and modification of the hardnesses further necessitated slight reparameterization of the remaining electrostatic and non-bonded parameters. The electronegativities of TIP4P-QDP and QDP-P1 were then reparameterized such that a single water molecule in vacuum minimizes to the experimental dipole moment of 1.85 D. Since the polarizabilities of QDP models in the condensed phase are higher than that of TIP4P-FQ, the Lennard–Jones parameters required minor modification to prevent over-polarization while still reproducing reasonable densities and energetics.

Table 1 Gas-phase, condensed-phase, and interfacial properties for TIP4P-FQ, TIP4P-QDP, and QDP-P1 water models

Property	TIP4P-FQ[a]	TIP4P-QDP	QDP-P1	Exper.
μ (debye)	1.85	1.85	1.85	1.85[b]
$\bar{\alpha}$ (Å^3)	1.12	1.4	1.4	1.47[c]
E_{dimer} (kcal/mol)	−4.50	−4.67	−4.44	−5.4 ± 0.7[d]
Dimer O–O length (Å)	2.92	2.91	2.98	2.98[d]
ρ_{liq} (g/cm^3)	1.0001 (0.0003)	0.9954 (0.0002)	0.9951 (0.0002)	0.997[e]
$\langle \mu_{\text{liq}} \rangle$ (Debye)	2.623 (0.001)	2.641 (0.001)	2.752 (0.001)	2.9 (0.6)[f]
ΔH_{vap} (kcal/mol)	10.49[g]	10.55 (0.12)	10.96 (0.12)	10.51[e]
$\langle \alpha_{\text{iso,liq}} \rangle$ Å^3	1.12[g]	1.309 (0.001)	1.323 (0.001)	1.34[h]
D_s (10^{-9} m^2/s) [m]	1.93 (0.05), 2.15	2.20 (0.04), 2.46	1.83(0.05), 2.04	2.30[i]
κ_T (10^{-10} Pa^{-1})	3.877 (0.098)	4.013 (0.062)	3.409 (0.051)	4.524[e]
C_p (cal/mol K)	21.0 (5.5)	16.4 (3.5)	18.5 (2.2)	18.0[e]
ε_∞	1.775, 1.592[g]	2.128	2.057	1.79[j]
ε	79. (8)[g]	85.8 (1.0)	97.6 (0.2)	78.[k]
$\Delta\Phi$ (kcal/mol)	−12.21 (0.05)	−11.98 (0.08)	−12.87 (0.05)	—
γ (dyne/cm)	72.7 (1.5)	71.0 (2.7)	81.2 (3.1)	71.9[l]

Values in parentheses denote the uncertainty in the property. Data from Bauer et al. [57]

[a] Reference [57], unless noted

[b] Reference [143]

[c] Reference [144]

[d] Reference [145]. Theoretical estimates from Mas et al. [146] suggest a value of 5.0 ± 0.1

[e] Reference [147]

[f] Reference [53]

[g] Reference [31]

[h] Estimated condensed-phase isotropic polarizability based on the gas-phase value of 1.47 Å^3 from reference [144] and assuming a 9% reduction in polarizability as deduced by Morita in reference [50]

[i] Reference [148]

[j] Reference [149]

[k] Reference [150]

[l] Reference [151]

[m] Values as calculated for a $N = 216$ system (left) and corrected for extrapolation to infinite system size (right)

The Lennard–Jones parameters were parameterized based on fitting to gas-phase water dimer binding energies and geometries (bond distances), condensed-phase density, and enthalpy of vaporization.

Condensed-phase properties computed using the TIP4P-QDP model include bulk liquid density from constant pressure MD simulations, enthalpy of vaporization, average condensed-phase molecular polarizability, diffusion constant, isothermal compressibility, heat capacity at constant pressure, and bulk dielectric constant. These properties are computed as discussed in Bauer et al. [57] and are shown in Table 1. We observe that without fitting explicitly to all of the properties in Table 1, the agreement between the predicted and experimental values is rather acceptable. We have applied this model to studies of the liquid-vapor coexistence curve [58] and ions at the liquid-vapor interface [59]. Studies using the Hirshfeld partitioning scheme [49, 52, 60–62] in conjunction with density functional theory have suggested the dynamic nature of polarizability for species such as methanol [62] and halides [52].

4 Development of CHEQ lipid bilayer force fields

Membranes and membrane-bound proteins are a vital part of biological systems. Membrane-bound proteins are involved in a number of physiological functions including but not limited to passive and active transport, signaling processes, and interfacial enzymatic processes [63]. Further emphasizing their importance, membrane-bound proteins have been found to make up approximately one-third of the human genome [64]. Equally important is the lipid environment within which these proteins function. Recent studies have explored structural properties of membranes as well as electrostatic properties such as the dielectric

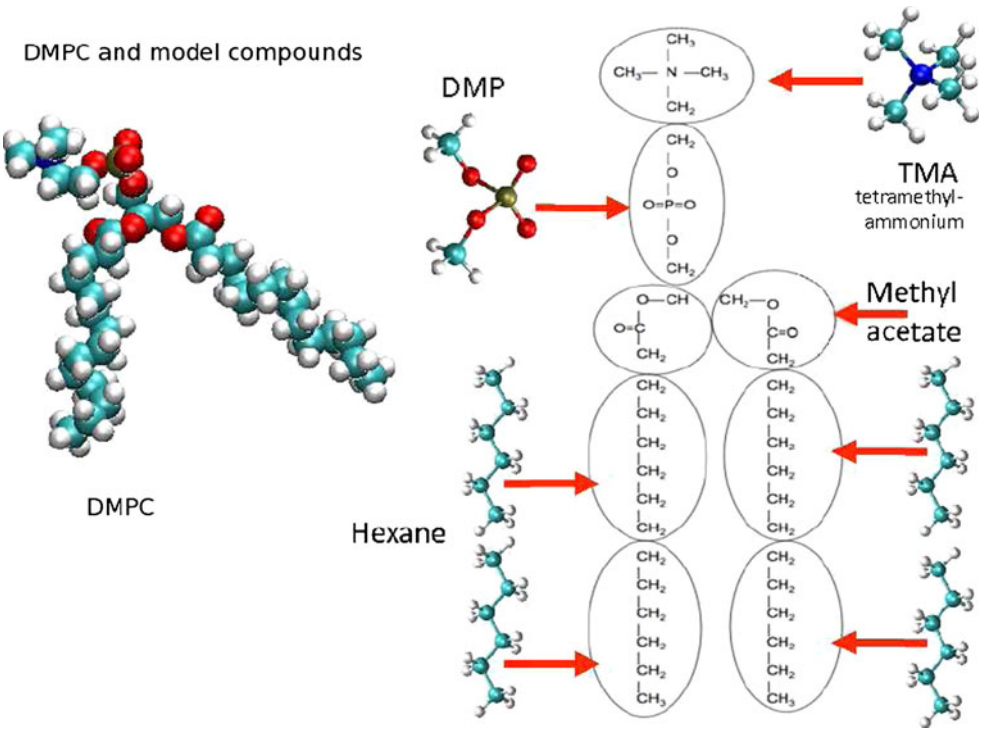

Fig. 2 Schematic of the partitioning of DMPC lipid molecule into small-molecule analogs for parameterization of the CHEQ lipid force field

variation within a bilayer [65], the interfacial potential [66], and the interactions of polar or charged amino acid side chains with hydrocarbon tails [67]. Experimental studies have also probed these properties in recent years. For example, structural properties of bilayers have been determined by X-ray and neutron scattering [68, 69] and nuclear magnetic resonance (NMR) spectroscopy [70], while the water penetration into the bilayer interior has been investigated via electron spin spectroscopy [71, 72] and X-ray scattering techniques [73]. However, even current state-of-the-art experimental measurements are not always able to provide the type of detailed atomic level resolution that would provide significant insights into the mechanisms of membrane systems. To this end, computational methods such as molecular dynamics and Monte Carlo simulations have been employed to study properties and processes in such systems at the atomic level [63, 67, 74–85].

Recently, we have developed non-additive, charge equilibration (CHEQ) force fields for lipid bilayers based on DMPC and DPPC as model lipid molecules [86, 87]. Using an approach of "building up" a lipid force field based from small-molecule model compounds, we constructed the lipid force field for saturated chain lipids using linear alkanes, dimethylphosphate, tetramethyl-ammonium, and methyl acetate as model compounds Fig. 2. Properties of the small-molecule analogs that were targeted included gas-phase electrostatic properties (dipole moments, charges, and molecular polarizabilities), gas-phase interaction energies and geometries of small-molecule compounds with water (using the TIP4P-FQ model as our solvent to which the force field is coupled), condensed-phase bulk liquid properties for alkanes (densities, vaporization enthalpies, self-diffusion constants, and relative torsional energetics), and hydration free energies of linear alkanes in water. The original CHEQ alkane force field [88] was refined using pair-specific Lennard–Jones interactions [89] in order to reduce the gain in free energy upon hydration predicted by the original force field. We discuss implications of this improvement in the next section. A range of lipid bilayer properties were computed following the parameterization process. These include bilayer structure (electron density profile, atomic number density profiles), deuterium order parameters, phosphate–nitrogen (P–N) vector orientation, and dipole potential.

4.1 Application of CHEQ lipid force fields

One interesting aspect of the CHEQ DMPC force field is increased water permeation into the hydrophobic core of the bilayer relative to the non-polarizable CHARMM27 and CHARMM27R force fields [86]. This is evidenced by an increased water number density beyond the carbonyl groups and reduced potential of mean force (PMF) for water entering the lipid tail region. The PMF calculated from water density profiles generated from long, unconstrained simulations of the solvated CHEQ DMPC bilayer suggests a 5-kcal/mol barrier for moving a water molecule from bulk to lipid interior [86]. Subsequent analysis using weighted histogram analysis method

(WHAM) suggests this barrier may as low as 4.5 kcal/mol [90].

Since the lipid groups were constructed from short chain alkane (hexane) parameters [43], the interactions of these alkanes with water have important implications for the interactions between water and lipids. Ongoing efforts towards refinement of the interactions of small molecules with water are of continued interest. One such study [89] presents refined interactions between small-chain alkanes and water, yielding alkane hydration free energies that are less favorable than those calculated using CHEQ Orig [86]. In the case of hexane, the reparameterization results in $\Delta G_{\text{hydration}} = 2.5 \pm 0.2$ kcal/mol (compared to the experimental value of $\Delta G_{\text{hydration}} = 2.550$ kcal/mol); this is approximately 0.7 ± 0.5 kcal/mol higher than the original parameterization [43]. The revised parameterization predicts a PMF barrier nearly 0.8 kcal/mol larger than the original parameterization. This is not surprising as qualitatively, an enhancement is expected from the less favorable interaction between water and the alkane. The range in values for the PMF barrier for different DMPC parameterizations (4.5–5.3 kcal/mol) is lower the values predicted from similar studies using non-polarizable models (5.4–13 kcal/mol) [86, 91–93].

5 Charge equilibration carbohydrate force fields

N-Acetyl-β -hexosaminides are common in nature. They constitute a broad spectrum of materials such as chitin [94] and extracellular matrix glycosaminoglycans [95, 96] and are an essential structural component of glycoproteins and glycolipids [97, 98]. They are also implicated in molecular recognition processes, acting as ligands for a variety of ribonucleases [99–101]. However, functions of poly-N-acetyl-glucosamine and glycosaminoglycans in cell signaling, development, and growth are not well understood, due to the lack of detailed information for the polymer solution [96, 102]. Vibrational spectroscopy [103–105], nuclear magnetic resonance (NMR) [106–110] spectroscopy, and X-ray crystallography [111–113] techniques are applied to investigate the solution structure of related polysaccharides. However, experimental approaches are often limited to certain molecular weight ranges and suffer from difficulties such as crystallization of glycoforms in polysaccharide solution systems.

Complementing experiment, computational methods are a powerful tool to study conformational properties of carbohydrates in solution [114]. Carbohydrate force fields developed for the CHARMM, AMBER, and GROMOS force fields [115, 116] enable MD simulations for polysaccharide solutions. Partly due to the sparsity of experimental data available for parameterization, development of classical force fields for these types of molecules has been relatively slow. Current state-of-the-art force fields for carbohydrate molecular simulations are primarily the work of Woods and co-workers throughout the past several decades [115]. Ha et al. [117] parameterized classical, non-polarizable force fields for the GROMOS platform. Palma et al. [118] later corrected the O–C–C–O term to revise the barrier of hydroxyl rotations (PHLB model). Kuttel, Brady, and Naidoo modified the PHLB parameter set for lower primary alcohol rotational barriers and referred to the force field as the Carbohydrate Solution Force Field (CSFF) [119–120]. Recently, MacKerell et al. [116] have developed atomistic force fields for carbohydrates building upon the CHARMM force field platform.

Recently, we have developed a polarizable force field based on the charge equilibration force field for an aminoglycan; this will be applied in future studies of protein-ligand binding free energetics using statistical mechanical free energy methods in conjunction with polarizable protein and ligand force fields. Polarizable, or non-additive, force fields for modeling of carbohydrate interactions with polar biological components (in particular proteins) may prove influential within the context of quantifying binding free energetics and structures of complexes of carbohydrates and proteins. By analogy to protein-drug binding and structure research, the use of non-additive interactions may allow a broader range of interaction energies so as to provide a larger separation between biologically relevant complexes (based on free energetics and structure) and weakly interacting, less-relevant complexes. Development of polarizable force fields for carbohydrates in general will complement the current efforts in a number of groups working on non-additive models for proteins, nucleic acids, small molecules, and lipid membranes, as well as ions and small-molecule condensed-phase systems. Work to date on protein-ligand binding studies suggests that polarization (in the most general sense taken to be the variation of molecular mechanics partial charges or electrostatic multipole moments with relative orientations of ligand and substrate) is important in both polar systems as well as situations where ionic species are involved [121–122]. In our continuing future work, we plan to apply polarizable models for the NAG system and compare to non-polarizable (additive) force fields in the context of free energetics of binding in the hen egg-white lysozyme system.

5.1 Parameterization of a charge equilibration force field for NAG

The philosophy we employ for deriving the charge equilibration force field for the monomer NAG is to fit to gas-phase first-principles (ab initio and density functional theory (DFT)) calculation-based properties such as

molecular polarizability, dipole moment, and interactions with water in various geometries. As a reference, gas-phase polarizability and dipole moment for NAG are calculated for the geometry optimized using density functional theory (DFT) with the B3LYP/6-311g(d,p) basis. Hardness parameters, η_i°, are determined by fitting to the molecular dipole polarizability (defined above). The augmented hardness matrix, $\mathbf{J}'$, is constructed using two charge normalization groups as shown in Fig. 3. Atomic electronegativities are then determined by fitting to DFT gas-phase charges and dipole moment according to the Merz–Singh–Kollman scheme. The force field gas-phase electrostatic properties are shown in Table 2 using the optimized electrostatic parameters (atom electronegativities and hardness parameters). Consistent with previous study [26], DFT method predicts higher polarizabilities than MP2 when using the same basis set. Higher level of theory predicts larger polarizability and DFT method shows similar polarizabilities when using aug-cc-pvDZ and aug-cc-pvTZ basis set. We note that the fitted gas-phase polarizability using the CHEQ model reproduces DFT and MP2 polarizability with the lower level of theory (6-311g(d,p)) and falls below the gas-phase reference values using larger basis set of aug-cc-pvDZ (14% for B3LYP and 15% for MP2). The absolute extent of reduction of molecular polarizabilities in the condensed phase still remains an ongoing avenue of research, with majority of scaling factors determined from empirical tuning of force field quality and associated stability of simulations using the force fields [36, 123].

After determining electrostatic parameters, solute–solvent interaction-derived non-bond repulsion–dispersion interaction parameters are determined. Solute–solvent nonbond interactions are determined by reproducing vacuum dimer energies and hydrogen binding distances. For reference, the optimized geometry of NAG–water heterodimer (Fig. 4) is obtained by DFT calculation using B3LYP/6-311g(d,p) level of theory. Table 3 shows optimized NAG–water interaction energy and geometry for the CHEQ force field, which is found to well-reproduce the reference first-principles results to at least comparable accuracy as the fixed-charge model. With this basic

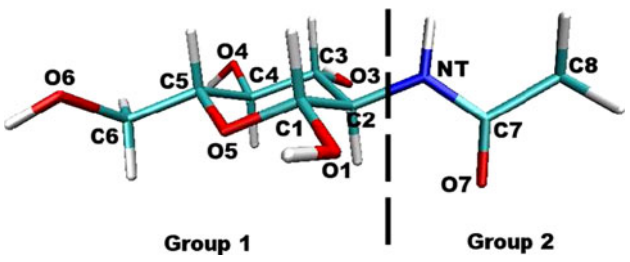

Fig. 3 Designation of charge conservation groups

Table 2 Electrostatic properties for NAG geometry optimized with B3LYP/6-311g(d,p) basis

	Polarizability/Å^3	Dipole moment/debye
B3LYP/6-311g(d,p)	17.29	5.1572
B3LYP/aug-cc-pvDZ	19.80	5.1604
B3LYP/aug-cc-pvTZ	19.82	5.1515
MP2/6-311g(d,p)	16.75	5.4377
MP2/aug-cc-pvDZ	19.46	5.4115
CHEQ	16.81	5.1160

NAG–water interaction model, we address in the next sections methods and results of condensed-phase molecular dynamics simulations of the NAG molecule (and its oligomers) in aqueous solution (Fig. 5).

5.2 Molecular dynamics simulations of polarizable protein-ligand complexes: hen egg-white lysozyme and NAG trimer

5.2.1 Molecular dynamics methodologies for simulations of hen egg-white lysozyme complexed with the NAG trimer

As an application, we performed molecular dynamics simulations of the complex between hen egg-white lysozyme (HEWL) and NAG trimer (NAG_3) with both the polarizable CHEQ and non-polarizable CHARMM carbohydrate [118] and protein [124] force fields. We used the CHEQ force field for proteins [36], water [31], and NAG_3 [125]. The simulations are the initial steps towards application of our models for protein-ligand absolute and relative binding free energy calculations using statistical mechanical approaches such as thermodynamic integration.

Two binding modes (ABD and BCD) of HEWL-$(NAG)_3$ complex are simulated independently. The ABC conformation is obtained from the X-ray crystal structure (PDB:1lzb). To construct the BCD structure, the carbohydrate residue at the A site is removed from the HEWL-$(NAG)_4$ X-ray structure bound in the ABCD site (PDB:1lzc). Each of the two starting structures is solvated in an octahedral water box. Bulk solution simulations were performed within the isothermal-isobaric ensemble (NPT) at 298 K and 1 bar. A constant temperature of 298 K was maintained with a Hoover thermostat [126–128], and constant pressure was maintained via a Langevin piston method [129]. Non-bonded interactions were switched to zero via a switching function from 10 to 12 Å. Conditionally convergent long-range electrostatic interactions were treated using the Smooth Particle Mesh Ewald [130] method with 24 grid points in each dimension and screening parameter of $\kappa = 0.32$. We performed ten

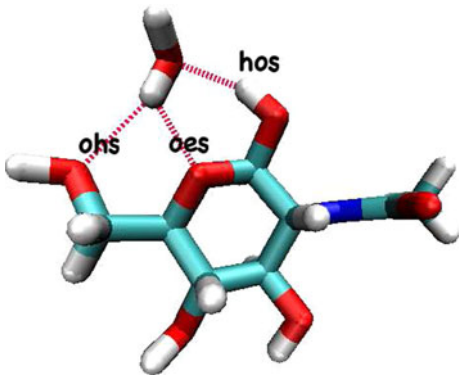

Fig. 4 Interactions between NAG and water in gas phase

Table 3 NAG–water gas-phase interactions and bond lengths

	E_{dimer} (kcal/mol)	R_{ohs} (Å)	R_{oes} (Å)	R_{hos} (Å)
B3LYP/6-311g(d,p)	−14.73	2.44	2.20	1.90
CHEQ	−14.10	2.85	2.18	1.99
PHLB	−9.55	2.82	1.98	2.06
PHLB-PSP	−13.51	2.87	1.60	1.81

Hydrogen bond types are described in Fig. 4

nanoseconds of molecular dynamics using a Verlet leap-frog integrator with timestep of 0.001 picoseconds (1 fs) using the CHARMM22 force field. Using the polarizable force field, we simulated the solvated X-ray structure (ligand at the ABC sites) for 8 ns and the one with $(NAG)_3$ bound to the BCD sites for 4 ns with timestep of 0.0005 ps (0.5 fs), the first 500 ps of which is considered as equilibration time. Charge degrees of freedom were maintained at 1K using a Nosé–Hoover bath; all charges were assigned to the same bath, and no local "hotspots" in charge were observed. Protein, water, and ligand charges degrees of freedom were assigned masses of 0.000095, 0.000069, and 0.0001 (kcal/mol $ps^2)/e^2$, respectively. Charge normalization was maintained by groups for the protein and ligand and over individual molecules for the water.

5.2.2 Analysis of MD simulations

HEWL X-ray crystallography studies suggest that $(NAG)_3$ binds at the ABC sites [131, 132] (Fig. 6). X-ray powder diffraction study [133] by Von Dreele, on the other hand, showed that $(NAG)_3$ occupies the ABC and BCD sites in the ratio of 35:65. Von Dreele [133] attributed the absence of BCD binding in the solid state to the hydrolysis at the CD site. We investigate the ABC and BCD complexes by two independent MD simulations starting from corresponding crystal binding structures as discussed above.

To evaluate the structural changes of the complex over the dynamic trajectory, the RMSD profiles for HEWL backbone Fig. 7 and $(NAG)_3$ heavy atoms Fig. 7 are computed with respect to the starting ABC (panels a and c) and BCD (panels b and d) crystal structures. The results for the CHEQ force field are in panels c and d; those for the non-polarizable are shown in panels a and b. The protein backbone atom RMSD behaves similarly using both force fields, with slightly larger drift from the crystal structure with the CHEQ model, particularly when $(NAG)_3$ binds to the BCD sites (Fig. 7, panel d); this implies that the protein structure changes to accommodate the ligand. Such conformational relaxation is not found in the simulation with the CHARMM22 force field. Here, we emphasize that the starting BCD conformation is obtained from the crystal structure with $(NAG)_4$, which may deviate from the exact BCD structure and require longer relaxation time for protein as the CHEQ model suggests (Fig. 7d). On the other hand, the ligand RMSD profile with larger fluctuations and larger RMSD values indicates that $(NAG)_3$ at the ABC sites is relatively flexible and undergoes more structural changes from the starting crystal structure (Fig. 7 panels a and c).

6 Summary

With the continuing advances in computational hardware [134, 135] and novel force fields constructed using quantum mechanics, the outlook for non-additive force fields is promising. Our work in the past several years has slowly demonstrated the utility of polarizable force fields, particularly those based on the charge equilibration formalism, for a broad range of physical and biophysical systems. We have constructed polarizable force fields for small molecules [36, 42–44, 125, 136, 137], proteins [37], lipids, and lipid bilayers [43, 86, 138–140] and recently have begun work on carbohydrate force fields [125]. The latter area has been relatively untouched by force field developers with particular focus on polarizable, non-additive interaction potential models.

With respect to polarizable force field development, one aspect that has been difficult to address has been the absolute nature of the reduction in condensed-phase intrinsic molecular polarizability; this is particularly important for polarizable formalisms that are more classical in nature. We have recently explored the effects of condensed-phase polarizability reduction as well as developed novel water potentials that begin to consider explicitly the dynamical variation of molecular polarizability with the local environment [57]. This is an important area for further development. We also note that charge transfer effects have largely been neglected in classical formalisms; the implications of charge transfer are now becoming more apparent, and the development of interaction potentials capable of

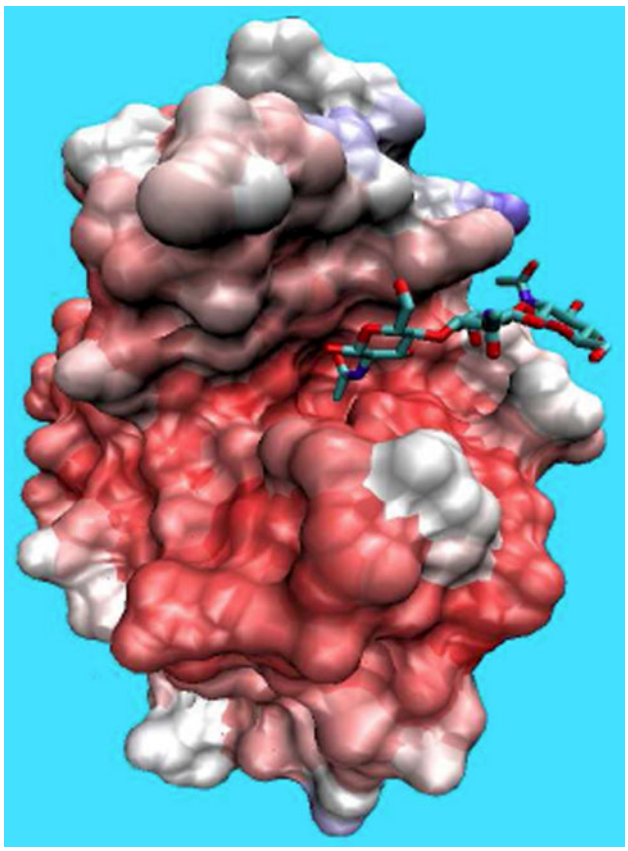

Fig. 5 Structure of the hen egg-white lysozyme complexed with NAG_3, taken from crystal structure PDBID:1LZB

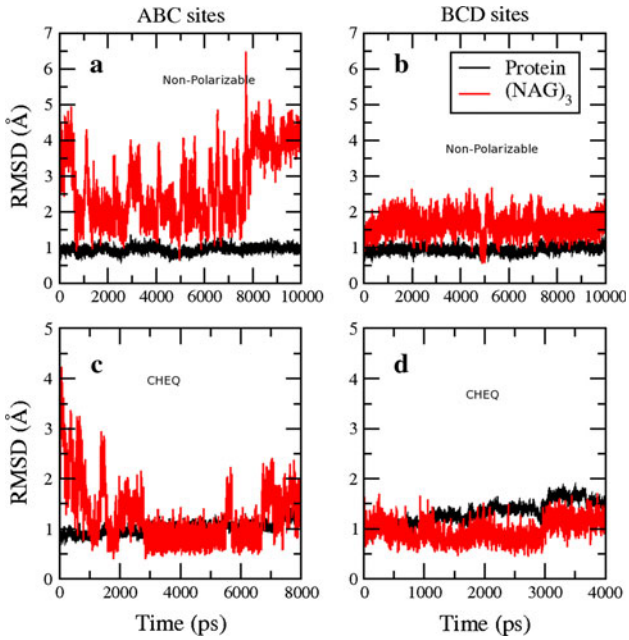

Fig. 7 Evolution of HEWL backbone and NAG_3 heavy-atom RMSD from crystal structure. *Left column* shows data for the ABC sites and *right column* for BCD sites. **a** and **b** Show results using the non-polarizable force field. **c** and **d** Show results using the CHEQ polarizable force field

Fig. 6 Binding site hydrogen bond topography of the hen egg-white lysozyme complexed with NAG_3 based on crystal structure PDBID:1LZB (*top panel* for sites ABC), and PDBID:1LZC (*bottom panel* for sites BCD)

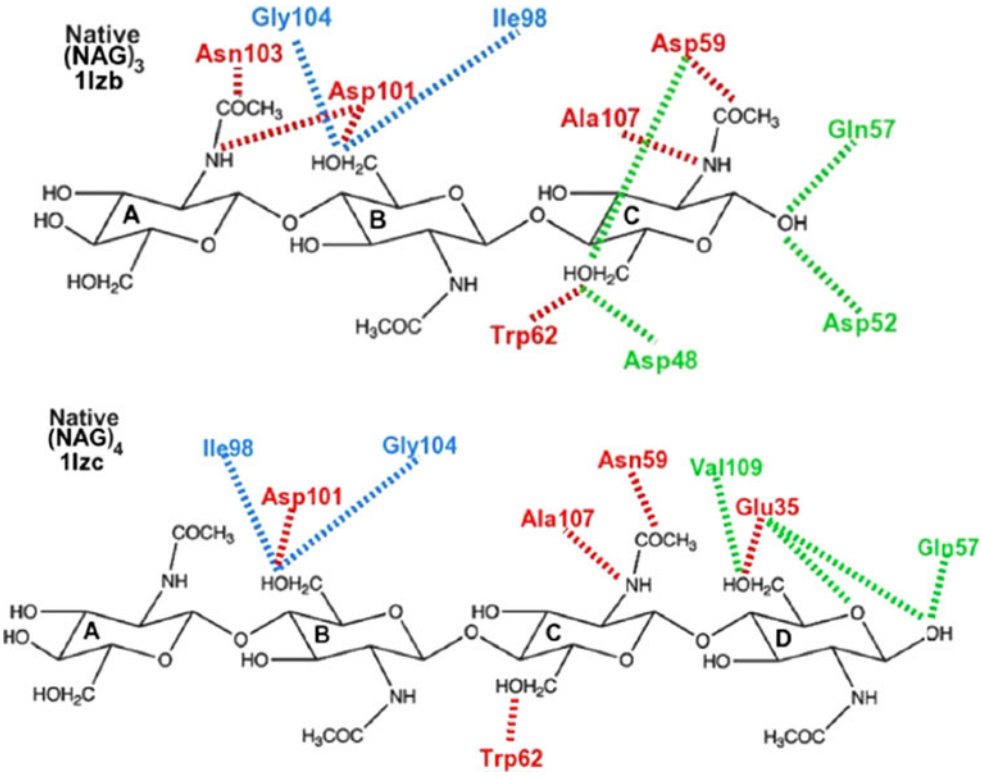

explicitly and dynamically including such effects is warranted, particularly for biophysical systems involving charge-dense ions.

With respect to biomacromolecular force fields, we have successfully constructed models for lipid molecules that we are now exploiting for molecular dynamics simulations of ion channels [138] and issues related to charge species in low-dielectric membrane environments [77, 141, 142]. Further development and refinement of such models continues aggressively in our lab.

We have also developed one of the first polarizable carbohydrate force fields for the NAG molecule and longer oligomers that are model systems for carbohydrate substrates to hen egg-white lysozyme, for instance. With the current efforts to include electronic polarization in classical force fields, we believe that this work establishes a platform on which to build more extensive polarizable force fields for an important class of biological macromolecules. We have successfully initiated studies of the hen egg-white lysozyme system complexed with its natural carbohydrate substrates and will progress to extended molecular dynamics simulations for absolute and relative binding free energy calculations in the near future.

References

1. Applequist J, Carl JR, Fung K (1972) J Am Chem Soc 94:2952–2960
2. Caldwell JW, Kollman PA (1995) J Phys Chem 99:6208–6219
3. Grossfield A, Ren P, Ponder JW (2003) J Am Chem Soc 125:15671–15682
4. Grossfield A (2005) J Chem Phys 122:024506
5. Jiao D, King C, Grossfield A, Darden TA, Ren P (2006) J Phys Chem B 110:18553–18559
6. Ponder JW, Wu C, Ren P, Pande VS, Chodera JD, Schnieders MJ, Haque I, Mobley DL, Lambrecht DS, DiStasio RA Jr, Head-Gordon M, Clark GNI, Johnson ME, Head-Gordon T (2010) J Phys Chem B 114:2549–2564
7. Ren P, Ponder JW (2002) J Comp Chem 23:1497–1506
8. Ren P, Ponder JW (2003) J Phys Chem B 107:5933–5947
9. Ren R, Ponder JW (2004) J Phys Chem B 108:13427–13437
10. Gresh N, Cisneros GA, Darden TA, Piquemal J-P (2007) J Chem Theory Comput 3:1960–1986
11. Thole BT (1981) Chem Phys 59:341–350
12. Anisimov VM, Lamoureux G, Vorobyov IV, Huang N, Roux B, MacKerell AD Jr (2005) J Chem Theory Comput 1:153–168
13. Lamoureux G, Roux B (2003) J Chem Phys 119:3025
14. Lamoureux G, MacKerell AD Jr, Roux B (2003) J Chem Phys 119:5185
15. Lamoureux G, Harder E, Vorobyov IV, Roux B, MacKerell AD Jr (2006) Chem Phys Lett 418:245–249
16. Lopes PEM, Lamoureux G, Roux B, MacKerell AD Jr (2007) J Phys Chem B 111:2873–2885
17. Vorobyov IV, Anisimov VM, AD MacKerell J (2005) J Phys Chem B 109:18988–18999
18. Vorobyov IV, Anisimov VM, Greene S, Venable RM, Moser A, Pastor RW, AD MacKerell J (2007) J Chem Theory Comput 3:1120–1133
19. Baker CM, Lopes PEM, Zhu X, Roux B, MacKerell AD Jr (2010) J Chem Theory Comput 6:1181–1198
20. Lamoureux G, Roux B (2006) J Phys Chem B 110:3308–3322
21. Yu H, Whitfield TW, Harder E, Lamoureux G, Vorobyov I, Anisimov VM, MacKerell AD Jr, Roux B (2010) J Chem Theory Comput 6:774–786
22. de Courcy B, Piquemal J-P, Garbay C, Gresh N (2010) J Am Chem Soc 132:3312
23. Devereux M, van Severen M-C, Parisel O, Piquemal J-P, Gresh N (2011) J Chem Theory Comput 7:138–147
24. Piquemal J-P, Chevreau H, Gresh N (2007) J Chem Theory Comput 3:824–837
25. Piquemal J-P, Williams-Hubbard B, Fey N, Deeth RJ, Gresh N, Giessner Prettre C (2003) J Comput Chem 24:1963
26. Piquemal J, Marquez A, Parisel O, Giessner-Prettre C (2005) J Comput Chem 26:1052
27. Piquemal J-P, Cisneros GA, Reinhardt P, Gresh N, Darden TA (2006) J Chem Phys 124:104101
28. Sanderson RT (1951) Science 114:670–672
29. Sanderson RT (1976) Chemical bonds and bond energy. Academic Press, New York
30. Rappe AK, Goddard WA (1991) J Phys Chem 95:3358–3363
31. Rick SW, Stuart SJ, Berne BJ (1994) J Chem Phys 101:6141–6156
32. Rick SW, Stuart SJ, Bader JS, Berne BJ (1995) J Mol Liq 65/66:31
33. Rick SW, Berne BJ (1996) J Am Chem Soc 118:672–679
34. Rick SW, Stewart SJ (2002) Reviews of computational chemistry. Wiley, New York, p 89
35. Rick SW (2001) J Chem Phys 114:2276–2283
36. Patel S, Brooks CL III (2004) J Comput Chem 25:1–15
37. Patel S, MacKerell AD Jr, Brooks CL III (2004) J Comput Chem 25:1504–1514
38. Patel S, Brooks CL III (2005) J Chem Phys 122:024508
39. Patel S, Brooks CL III (2006) Mol Simul 32:231–249
40. Olano LR, Rick SW (2005) J Comput Chem 26:699–707
41. Warren GL, Davis JE, Patel S (2008) J Chem Phys 128:144110
42. Zhong Y, Warren GL, Patel S (2007) J Comp Chem 29:1142–1152
43. Davis JE, Warren GL, Patel S (2008) J Phys Chem B 112:8298–8310
44. Bauer BA, Patel S (2008) J Mol Liq 142:32–40
45. Illingworth CJ, Domene C (2009) Proc R Soc A 465:1701–1716
46. Nalewajski RF, Korchowiec J, Zhou Z (1988) Int J Quant Chem 22:349–366
47. Chelli R, Procacci P, Righini R, Califano S (1999) J Chem Phys 111:8569–8575
48. Car R, Parrinello M (1985) Phys Rev Lett 55:2471–2474
49. Krishtal A, Senet P, Yang M, Van Alsenoy C (2006) J Chem Phys 125:034312
50. Morita A (2002) J Comput Chem 23:1466–1471
51. Schropp B, Tavan P (2008) J Phys Chem B 112:6233–6240
52. Bauer BA, Lucas TR, Krishtal A, van Alsenoy C, Patel S (2010) J Phys Chem A 114:8984–8992
53. Badyal YS, Saboungi M, Price DL, Shastri SD, Haeffner DR, Soper AK (2000) J Chem Phys 112:9206–9208
54. Kuo IW, Mundy CJ, Eggimann BL, McGrath MJ, Siepmann J, Chen B, Vieceli J, Tobias DJ (2006) J Phys Chem B 110:3738–3746
55. Silvestrelli PL, Parrinello M (1999) Phys Rev Lett 82:3308–3311
56. Sprik M (1991) J Chem Phys 95:6762–6769
57. Bauer BA, Warren GL, Patel S (2009) J Chem Theory Comput 5:359–373
58. Bauer BA, Patel S (2009) J Chem Phys 131:084709
59. Bauer BA, Patel S (2010) J Chem Phys 132:8107–8117

60. Hirshfeld FL (1977) Theor Chim Acta 44:129–138
61. Bultinck P, Van Alsenoy C, Ayers PW, Carbo-Dorca R (2007) J Chem Phys 126:144111
62. Krishtal A, Senet P, Van Alsenoy C (2008) J Chem Theory Comput 4:426–434
63. Roux B, Allen T, Berneche S, Im WQ (2004) Rev Biophys 37:15–103
64. Wallin E, Von Heijne G (1998) Protein Sci 7:1029–1038
65. Stern HA, Feller SE (2003) J Chem Phys 118:3401–3412
66. Wang L, Bose PS, Sigworth F (2006) J PNAS 103:18528–18533
67. MacCallum JL, Bennett WFD, Tielman DP (2008) Biophys J 94:3393–3404
68. Kučerka N, Liu Y, Chu N, Petrache HI, Tristram-Nagle S, Nagle JF (2005) Biophys J 88:2626–2637
69. Kučerka N, Nagle JF, Sachs JN, Feller SE, Pencer J, Jackson A, Katsaras J (2008) Biophys J 95:2356–2367
70. Petrache HI, Dodd SW, Brown MF (2000) Biophys J 79:3172–3192
71. Marsh D (2002) Eur Biophys J 31:559–562
72. Erilov DA, Bartucci R, Guzzi R, Shubin AA, Maryasov AG, Marsh D, Dzuba SA, Sportelli L (2005) J Phys Chem B 109:12003–12013
73. Mathai JC, Tristram-Nagle S, Nagle JF, Zeidel ML (2008) J Gen Physiol 131:69–76
74. Allen TW, Bastug T, Kuyucak S, Chung S-H (2003) Biophys J 84:2159–2168
75. Berneche S, Roux B (2002) Biophys J 82:772–780
76. Allen TW, Andersen OS, Roux B (2004) PNAS 101:117–122
77. Dorairaj S, Allen TW (2007) PNAS 104:4943–4948
78. Aliste MP, Tieleman DP (2005) BMC Biochem 6:30
79. Tieleman DP, MacCallum JL, Ash WL, Kandt C, Xu Z, Monticelli LM (2006) J Phys Condens Matter 18:S1221–S1234
80. Xu Z, Luo HH, Tieleman DP (2007) J Comput Chem 28:689–697
81. Feller SE (2000) Curr Opin Colloid Interface Sci 5:217–223
82. MacCallum JL, Tieleman DP (2006) J Am Chem Soc 128: 125–130
83. Pandit SA, Bostick D, Berkowitz ML (2004) Biophys J 86: 1345–1356
84. Berkowitz ML, Bostick DL, Pandit SA (2006) Chem Rev 106:1527–1539
85. Siu SWI, Vacha R, Jungwirth P, Bockmann RA (2008) J Chem Phys 128:125103
86. Davis JE, Rahaman O, Patel S (2009) Biophys J 96:385–402
87. Davis JE, Patel S (2009) J Phys Chem B 113:9183–9196
88. Patel S, Brooks CL III (2006) J Chem Phys 124:204706
89. Davis JE, Patel S (2010) Chem Phys Lett 484:173–176
90. Bauer BA, Lucas TR, Meninger D, Patel S (2011) Chem Phys Lett. doi:10.1016/j.cplett.2011.04.052
91. Orsi M, Sanderson WE, Essex JW (2009) J Phys Chem B 2009:12019–12029
92. Sugii T, Takagi S, Matsumoto Y (2005) J Chem Phys 123: 184714
93. Jedlovszky P, Mezei M (2000) J Am Chem Soc 122:5125–5131
94. Austin PR, Brine CJ, Castle JE, Zikakis JP (1985) Science 212:749
95. Alberts B, Johnson A, Lewis J, Raff M, Roberts K, Walter P (2002) Molecular biology of the cell. Garland Science, New York
96. Fukuda M, Hindsgaul O (1994) Molecular glycobiology. IRL Press at Oxford University Press, Oxford
97. Varki A (2006) Cell 126:841
98. Weerapana E, Imperiali B (2006) Glycobiology 16:91R
99. Haltiwanger RS, Hill RL (1986) J Biochem 261:15696
100. Lew DB, Songu-Mize E, Pontow SE, Stahl PD, Rattazzi MC (1994) J Clin Invest 94:1855
101. Arkar K, Sarkar HS, Kole L, Das PK (1996) Mol Cell Biochem 156:109
102. Almond A (2005) Carbohydr Res 340:907
103. Kovacs A, Nyerges B, Izvekov V (2008) J Phys Chem B 112:5728
104. Paolantoni M, Sassi P, Morresi A, Santini S (2007) J Chem Phys 127:24504
105. Gallina ME, Sassi P, Paolantoni M, Morresi A, Cataliotti RS (2006) J Phys Chem B 110:8856
106. Bush CA, Martin-Pastor M, Imberty A (1999) Annu Rev Biophys Biomol Struct 28:269
107. Peters T, Binto BM (1996) Curr Opin Struct Biol 6:710
108. Almond A, DeAngelis PL, Blundell CD (2006) J Mol Biol 358:1256
109. Blundell CD, DeAngelis PL, Day AJ, Almond A (2004) Glycobiology 14:999
110. Prestegard JH, Al-Hashimi HM, Tolman JRQ (2000) Res Biophys 33:371
111. Kuroki R, Ito Y, Kato Y, Imoto T (1997) J Biol Chem 272:19976
112. Maenaka K, Matsushima M, Song H, Sunada F, Watanabe K, Kumagai I (1995) J Mol Biol 247:281
113. Ose T, Kuroki K, Matsushima M, Kumagai I (2009) J Biochem 146:651
114. Vilegenthart, JFG, Woods, RJ (eds) (2006) NMR spectroscopy and computer modeling of carbohydrates: recent advances. American Chemical Society, Washington
115. Woods RJ, Dwek RA, Edge CJ (1995) J Phys Chem 99:3832
116. Guvench O, Greene SN, Kamath G, Brady JW, Venable RM, Pastor RW, MacKerell AD Jr (2008) J Comp Chem 29:2543
117. Ha SN, Giammona A, Field M, Brady JW (1988) Carbohydr Res 180:207
118. Palma R, Himmel ME, Liang G, Brady JW (2001) In: ACS symposium series: glycosyl hydrolases in biomass conversion. American Chemical Society, Washington, p 112
119. Naidoo KJ, Kuttel MJ (2001) Comput Chem 22:445
120. M Kuttel JWB, Naidoo KJ (2002) J Comput Chem 23:1236
121. Jiao D, Golubkov PA, Darden TA, Ren P (2008) Proc Natl Acad Sci 105:6290–6295
122. Khoruzhii O, Donchev AG, Galkin N, Illarionov A, Olevanov M, Ozrin V, Queen C, Tarasov V (2008) Proc Natl Acad Sci 105:10378–10383
123. Patel S, MacKerell AD Jr, Brooks CL III (2004) J Comput Chem 25:1504
124. MacKerell AD Jr et al (1998) J Phys Chem B 102:3586–3616
125. Zhong Y, Bauer BA, Patel S (2011) J Comput Chem (in revision)
126. Nosé S (1984) J Chem Phys 81:511–519
127. Nosé S (1984) Mol Phys 52:255–268
128. Nosé S (1990) J Phys Condens Matter 2:SA115–SA119
129. Allen MP, Tildesley DJ (1987) Computer simulations of liquids. Clarendon, Oxford
130. Darden T, York D, Pedersen L (1993) J Chem Phys 98:10089–10092
131. Cheetham JC, Artymiuk PJ, Phillips DC (1992) J Mol Biol 224:613
132. Maenaka K, Mastushima M, Song H, Sunada F, Watanabe K, Kumagai I (1995) J Mol Biol 247:281
133. von Dreele RB (2004) Acta Cryst D 61:22
134. Bauer BA, Davis JE, Taufer M, Patel S (2011) J Comput Chem 32:375–385
135. Ganesan N, Bauer BA, Lucas TR, Patel S, Taufer M (2011) J Comput Chem (submitted, in revision)
136. Zhong Y, Patel S (2009) J Phys Chem B 113:767–778
137. Zhong Y, Patel S (2010) J Phys Chem B 114:11076–11092

138. Patel S, Davis JE, Bauer BA (2009) J Am Chem Soc 131:13890–13891
139. Patel S, Zhong Y, Bauer BA, Davis JE (2009) J Phys Chem B 113:9241–9254
140. Lucas TR, Bauer BA, Patel S (2011) J Comput Chem (in revision)
141. Vorobyov I, Allen TW (2010) J Chem Phys 132:185101
142. Schow EV, Freites JA, Cheng P, Bernsel A, von Heijne G, White SH, Tobias DJ (2011) J Membr Biol 239:35–48
143. Clough SA, Beers Y, Klein GP, Rothman LS (1973) J Chem Phys 59:2254–2259
144. Murphy WF (1977) J Chem Phys 67:5877–5882
145. Odutola JA, Dyke TR (1980) J Chem Phys 72:5062–5070
146. Mas EM, Bukowski R, Szalewicz K, Groenenboom GC, Wormer PES, van der Avoird A (2000) J Chem Phys 113:6687–6701
147. Lide, DR (eds) (1997) CRC handbook of chemistry and physics, 77th edn. CRC, Boca Raton
148. Krynicki K, Green CD, Sawyer DW (1978) Discuss Faraday Soc 66:199–208
149. Buckingham AD (1956) Proc R Soc Lond Ser A 238:235–244
150. Watanabe K, Klein ML (1989) Chem Phys 131:157–167
151. Cini R, Logio G, Ficalbi A (1972) J Colloid Interface Sci 41:287–297